Brune, S., Babeyko, A. Y., Gaedicke, C., Ladage, S. (2010): Hazard assessment of underwater landslide-generated tsunamis: a case study in the Padang region, Indonesia. - Natural Hazards, 53, 2, 205-218

DOI: 10.1007/s11069-009-9424-x

Hazard assessment of underwater landslide generated tsunamis: a case study for the Padang region, Indonesia

Sascha Brune [1*], Andrey Y. Babeyko [1], Christoph Gaedicke [2], Stefan Ladage [2]

[1] *GFZ German Research Centre for Geosciences, Potsdam, Telegrafenberg, 14473 Potsdam, Germany*
[2] *Federal Institute for Geosciences and Natural Resources (BGR), Stilleweg 2, 30655 Hannover, Germany*
[*] *Corresponding author. e-mail: brune@gfz-potsdam.de*

Abstract

Submarine landslides can generate local tsunamis with high run-ups, posing a hazard to human lives and coastal facilities. Both ancient (giant Storegga slide off Norwegian coast, 8200 B. P.) and recent (Papua New Guinea, 1998) events show high potential danger of tsunamigenic landslides and the importance of mitigation efforts. This contribution presents newly discovered landslides 70 km off Padang (Western Sumatra, Indonesia), based on recent bathymetry measurements. This highly populated city with over 750.000 inhabitants exhibits high tsunami vulnerability due to its very low elevation. We model tsunamis that might have been induced by the detected landslide events. Estimations of run-up heights extrapolated from offshore tsunami amplitudes for Padang and other locations in the northern Mentawai fore-arc basin yield maximum values of about 3 m. We also provide a systematic parametric study of landslide-induced tsunamis which allows to distinguish potentially dangerous scenarios for Padang. Inside the fore-arc basin, scenarios involving volumes of 0.5 to 25 km³ could endanger Padang. Apart from slide volume, the hazard distribution mainly depends on three landslide parameters: distance to Padang, water depth in the generation region and slide direction.

Keywords: Submarine landslide; Tsunami; Numerical modeling; Indonesia; Padang; Hazard assessment

1. Introduction

Large tsunamis can arise from submarine earthquakes or landslides, threatening human lives and infrastructures in coastal areas. Large parts of Indonesia are particularly prone to tsunami danger as being located adjacent to the Sunda subduction zone. Here, the Indo-Australian plate subducts beneath the Sunda continental plate at convergence rates of about 6 cm/yr (Chlieh et al. 2008). The continuing accumulation of stress leads to a high earthquake potential (Hamzah et al. 2000). In 1994, an earthquake generated a tsunami off Eastern Java that reached a maximal run-up of 14 m (Tsuji et al. 1995a). Ten years later, the Great Sumatra-Andaman Earthquake of December, 2004 generated a tsunami that inundated the coasts of Indonesia, Thailand, Sri Lanka and India, but also of several East African countries (Synolakis and Kong 2006). In 2006, Central Java experienced an earthquake tsunami with maximum inundation heights of more than 20 m (Lavigne et al. 2007; Fritz et al. 2007). But even moderate earthquakes can induce tsunamis by triggering submarine mass failures. The most prominent event of this kind is the 1998 Papua New Guinea tsunami, where an underwater slump of 4 km³ led to

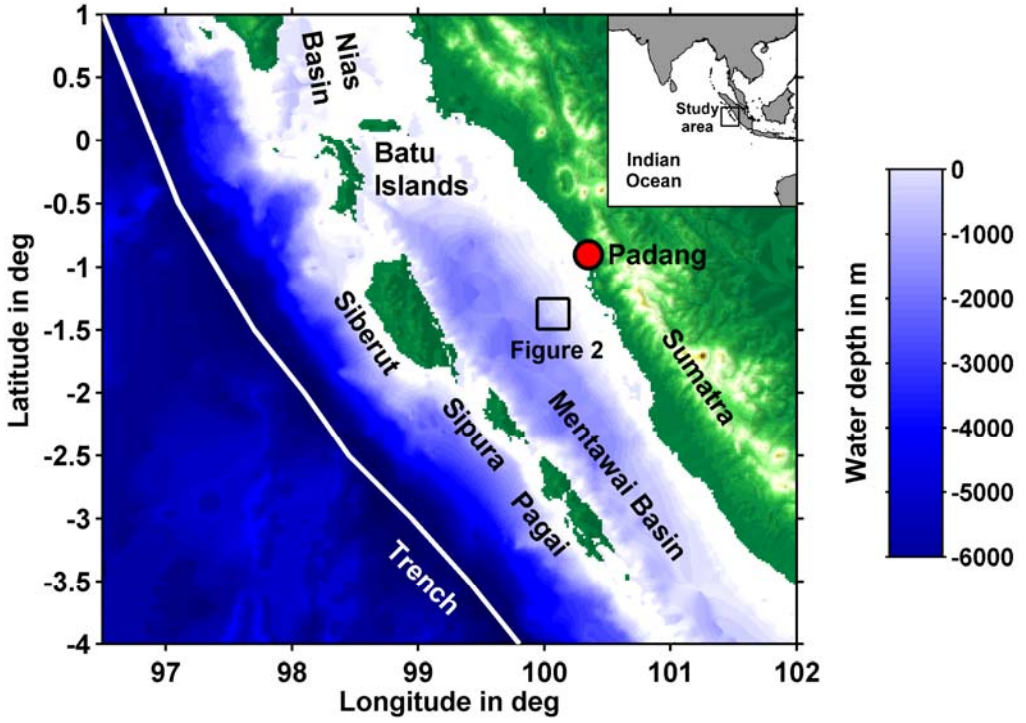

Figure 1 *Overview map.*

maximum wave heights of 15 m at the 30 km distant coast line (Tappin et al. 2001; Sweet and Silver 2003). In Indonesia, the involvement of submarine landslides has been proposed for the 1979 tsunami at Lomblen Island as well as for the 1992 event at the northern coast of Flores Island (Tsuji et al. 1995b; Rynn 2002). Bathymetry measurements at the trench off Sumba Island revealed large landslides with estimated volumes of up to 95 km³ (Brune et al., in prep.). Whether the extreme run-up at Nusa Kambangan during the Central Java tsunami of 2006 should be attributed to a landslide, is a current matter of debate (Matsumoto 2007). West of Sumatra, submarine slides have been discovered during the cruises that followed the 2004 earthquake. Moran and Tappin (2006) describe a blocky debris avalanche at the foot of the accretionary prism west of the Aceh basin. The largest out-runner block measures 2 km in length and 1 km in width, however, it was shown that the event was not connected to the Sumatra earthquake.

In recent years, numerical modeling has become a useful tool to estimate the hazard due to submarine landslides. Several landslide tsunami models have been developed and applied anywhere in the world. For detailed descriptions, see Harbitz (1992), Imamura and Imteaz (1995), Tinti et al. (1997), Grilli and Watts (1999), Pelinovsky (2001), Lynett and Liu (2002) and references therein.

In this study, we investigate the hazard potential of landslide-generated tsunamis near the city of Padang, situated in West Sumatra at the northern part of the Mentawai fore-arc basin. Padang, with more than 750.000 inhabitants, is one of the largest cities of Sumatra. As it is located on low coastal plains, its vulnerability in the case of tsunami arrival is particularly high. Moreover, recent studies indicate an elevated probability of a large

earthquake in this region due to long-period strain accumulation by plate coupling (Chlieh et al. 2008) and Coulomb stress transfer after the 2004 and 2005 Sumatran earthquakes (McCloskey et al. 2008).

After a short description of the geological background, we present new high-resolution bathymetry data collected by the RV "Sonne" in 2006 exhibiting three landslide events inside the Mentawai Basin, 70 km off Padang. Derived landslide parameters are then employed for the numerical modeling of potentially generated tsunamis. Finally, we provide a systematic parametric study of landslide-induced tsunamis offshore Padang. The idea of this study is to identify landslide and tsunami scenarios which might be dangerous for the city of Padang.

2. Geological background

Our study area comprises the northern part of the Mentawai Basin which is one of several depositional basins located off Sumatra along the Sunda Arc (Figure 1). The latter is a classical convergent margin system that stretches over 5000 km from Timor in the southeast to Burma in the north. The arc is the geological expression of the convergence between the Indo-Australian and the Sunda Plate where oceanic lithosphere is being subducted beneath the Indonesian island arc as well as the Andaman and Nicobar Islands. The Mentawai Basin is the widest and longest fore-arc basin off Sumatra extending over 550 km from the southern tip of Sumatra to the Batu Islands in the north. To the west, it is bordered by the outer arc high that, merging above sea level, forms the Mentawai Islands (from Siberut over Sipura and Pagai to Enggano). The basin has a maximum width of 140 km between the island of Siberut and Sumatra. The Batu Islands separate the Mentawai Basin from the northerly located Nias Basin. West of the Sunda Strait the outer arc high broadens forming a slightly shallower ridge that separates the Mentawai Basin from the West Java Basin (Susilohadi et al. 2005).

Basin geometry is uniform in the entire basin. The depth of the sea floor reaches 1700 m in the Mentawai Basin off Padang. The sediments are up to 4.8 s two-way travel time (TWT) thick, which, assuming a sound speed of 1500 m/s (Hamilton 1985) corresponds to approximately 3600 m. The minimum thickness along the basin axis is 3.5 s TWT, or roughly 2600 m. The acoustic basement underlying the sedimentary succession dips from the Sumatran shelf to the south-west where the maximum depth is reached close to the outer arc high.

The basin fill consists of terrigenous hemipelagic sediments with parallel, highly continuous reflections of medium to strong amplitude. Within the basin fill, some minor unconformities occur. Along the Sumatra margin multiphase sea level changes are documented in prograding and retrograding delta complexes below the shelf. This delta wedge gives evidence that Sumatra is the main source area for sediments deposited in the Mentawai Basin. Slump structures and debris flows exhibited in multi-channel seismic profiles give evidence for ancient slope failures in these delta complexes (Neben and Gaedicke 2006).

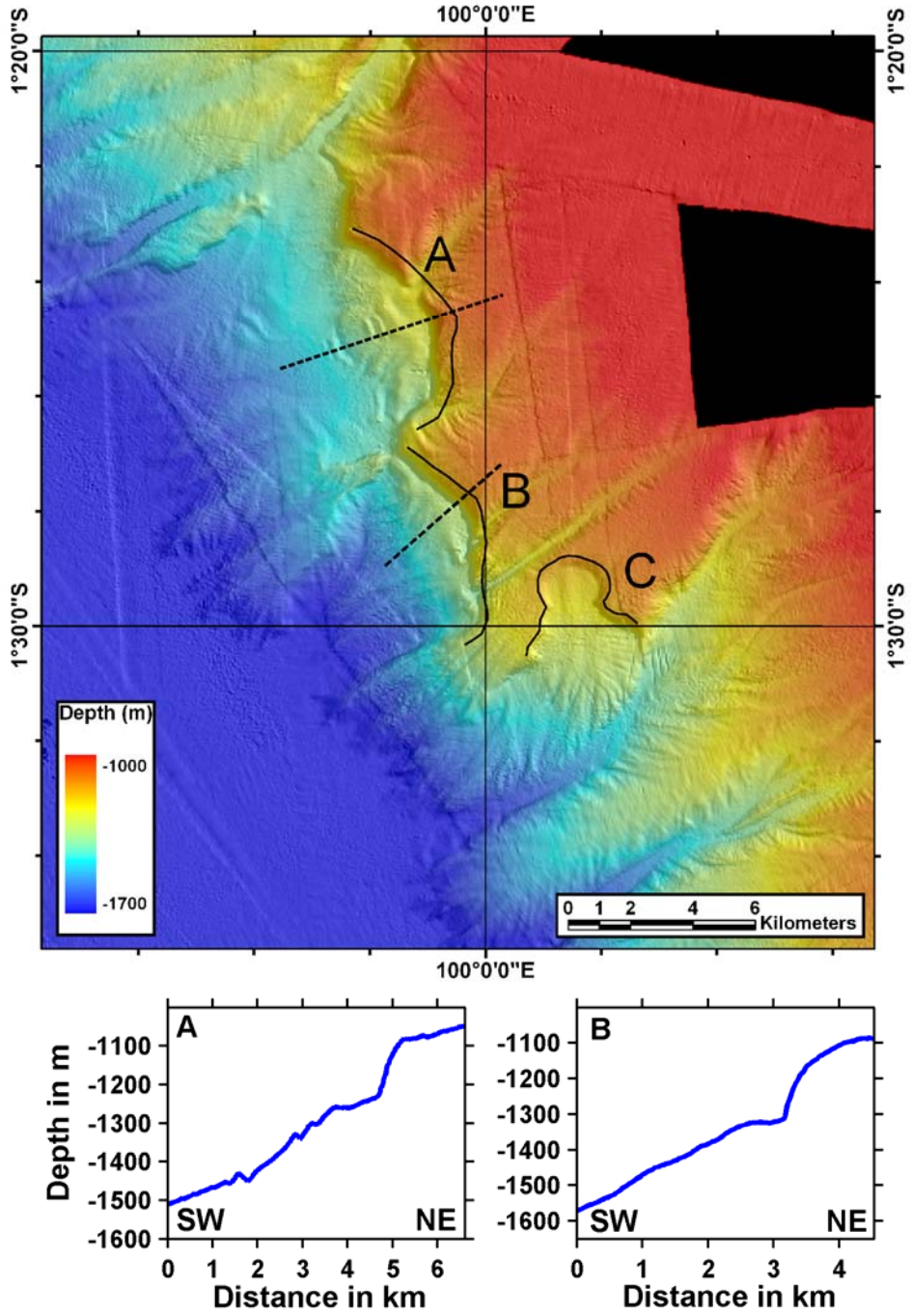

Figure 2 *Bathymetry map of the submarine landslides. Solid black lines are head scarp interpretations. Dashed lines indicate locations of cross sections profiles of the events A and B shown below (directed from southwest to northeast). For the location of this map with respect to the surrounding area, please refer to Figure1.*

Ground motions during earthquakes pose the main trigger for submarine landslides (Masson et al. 2006). The Mentawai segment of the Sumatra subduction zone is capable of producing earthquakes with magnitudes bigger than 8.5. This happened both in 1797 and in 1833 generating a large tsunami (Natawidjaja et al. 2006). It is current matter of debate, whether a comparable event in this area could recur soon (McCloskey et al. 2008; Chlieh et al. 2008). In September 2007, a series of earthquakes occurred west of Bengkulu, within the fault area of the 1833 rupture. Although magnitudes of 8.4 and 7.9 were reached, these events did not release the stress that was accumulated since 1833 (Lorito et al. 2008; Borrero et al. 2007; Chlieh et al. 2008).

3. Slide descriptions

During the SO189 cruise of the RV Sonne, west of Sumatra, new multibeam bathymetry data was collected. Horizontal resolution in the fore-arc basins amounts to about 50 m. The new data reveals a landslide site at the foot of the eastern fore-arc basin slope, within 70 km distance to the city of Padang. The site consists of three sub-events exhibiting concave head scarps up to 150 m height (Figure 2). In the following, we will refer to them as slide A, B, and C, respectively.

At the foot of slide A, compressional features can be clearly observed in the bathymetry. We interpret them to be the lower end of the failure surface and suggest rotational slumping as a corresponding failure mechanism. The slump width and length amount to 6 km and 3 km, respectively (Table 1). By comparing disturbed and adjacent undisturbed profiles, the thickness of the slump was estimated to be 100 m. Event B shows similar parameters to slide A, except for a shorter length of approximately 2 km. The last sub-event, slide C, which is located at south-east, is much smaller than the previous ones. The height of the head scarp amounts to 50 m. Furthermore, the head wall is divided into several segments indicating that failure took place in multiple stages.

Available parametric sediment echosound data lines cross the slide locations A and B (not shown here). Within the slide areas, echosound data display undisturbed, stratified sediments. The penetration depth in the sediments is 0.06 ms TWT which (if we assume a sound speed of 1500 m/s, Hamilton 1985) corresponds to 50 m. Thus, the failure surface lies deeper than 50 m which is in agreement with our previous height estimation of 100 m. As the sediment echosound lines are located perpendicular to the slide directions, no information can be obtained about the rotation angle of the slumps. Side scan images have been evaluated, as well. They clearly show head scarps, but do not display any additional details.

Dating of submarine landslides, based only on bathymetric data is difficult. The scars seem relatively fresh, however, slide A and B exhibit small erosional features at the canyon mouths. Mean sedimentation rates of 7 cm/kyr during the last 300.000 years have been estimated in the Sunda strait (Lückge et al. 2009). But as we do not see sediment cover, age estimation is not possible.

	Slide A	Slide B	Slide C
Width w (km)	6	6	2.5
Length (km)	3	2	2.5
Height (m)	100	100	50
Volume (km³)	0.7	0.5	0.1
Depth (m)	1300	1300	1300
Travel Distance (km)	2	1.5	2
Mean local slope angle (°)	5	6.5	3
Initial wave height η_{2HD} (m)	2.0	2.1	0.2
Characteristic wave length λ (km)	7	5	9
Characteristic time t_0 (s)	60	40	70

Table 1 *Geometric landslide parameters. For volume estimations, a parabolic slide form is assumed. The tsunami hot start parameters (initial wave height, wave length and characteristic time) have been calculated according to Watts et al. (2005).*

4. Modeling of induced tsunamis

4.1 Methods

We model landslide-generated tsunamis in three distinct stages: generation, propagation and run-up. Since the common shallow-water approximation is not valid for the generation phase (the ratio of slide length to submergence depth is too small, e.g., Lynett and Liu, 2002), we follow the wavemaker technique of Grilli and Watts (2005) and Watts et al. (2005). Combining physical arguments and wave tank experiments, produced a set of semi-empirical equations for two horizontal dimensions (2HD) that yield the initial tsunami wave height η_{2HD}, wave length λ and a characteristic time t_0. According to the wavemaker technique, the influence of a submarine mass movement on the sea surface can be approximated by an initial wave distribution. During the acceleration phase of a slide, the most important part of wave energy is used for the build-up of the wave. When the slide does not accelerate anymore, i.e. after the characteristic time t_0, this potential energy is transformed into kinetic energy. We construct the initial wave distribution by analogy to Synolakis et al. (2002) and Watts et al. (2005): The first-order impact of a submarine mass failure on the sea surface consists of vertical uplift in direction of the movement and subsidence in backward direction. First, consider a slide for one horizontal dimension (1HD). We approximate the elevated and the subsided water surface using two Gaussians. The amplitude of each curve is the initial wave height η_{1HD}, and its width equals to the characteristic wave length λ. Their center points are located at a distance of one wave length from each other. Thus, the initial form with wave length 2λ collapses into two wave trains of wave length λ moving in opposite directions. This initial waveform would be feasible for 1HD simulations. 2HD formulation additionally requires a waveform description in the direction perpendicular to the slide movement. Watts et al. (2005) proposed a solitary-like extrapolation proportional to $\mathrm{sech}^2(3 \cdot y/(w+\lambda))$, where w is the slump width and y the coordinate perpendicular to the slide direction. Hereby, due to mass conservation, the wave amplitude has to be modified. Watts and his coworkers suggest the multiplication of η_{1HD} with $w/(w+\lambda)$, to obtain the 2HD wave amplitude η_{2HD}.

The values of η_{2HD}, λ and t_0 for slides A, B, and C are listed in Table 1.

The scope of application for this method is discussed in Watts et al. (2005). Involved slope angles must be smaller than 30° which is obviously fulfilled (Table 1 and 2). Furthermore, the ratio of initial submergence depth to slide length must be larger than 0.06 in order to avoid wave breaking effects, which are not included in the model. For our slides A to C, this ratio amounts to 0.4, 0.7, and 0.5, clearly satisfying the condition.

Alternative 2HD formulations exist that use a submerged slide body which dynamically builds up a surface wave. They have been implemented in either shallow-water (Harbitz 1992) or Boussinesq approximation (Lynett and Liu 2005). Although these formulations allow to implement specific features of a landslide, their validity is restricted by submergence depth and length of a slide. As shown by Lynett and Liu (2002), shallow-water models of dynamic landslides are only feasible, if the ratio of slide length to submergence depth is larger than 30. More accurate Boussinesq formulations are valid if the ratio exceeds 7 (these figures hold true for symmetrical slide geometries, as discussed in Lynett and Liu 2002). In our case though, the length to depth ratios are clearly below the threshold: 2.3, 1.5 and 1.9 for slide A to C, respectively. For a detailed numerical study of deep or small slides, the usage of fully 3D, or 2HD-vertical models based on Reynolds averaged Navier–Stokes equations (RANS) (Yuk et al. 2006) or fully nonlinear potential flow (FNPF) (Grilli et al. 2002) would be promising. These models would allow the usage of more slide parameters concerning geometry, rheology and movement history. However, these parameters are unknown in our case, and we do not want to make any unconfident assumptions. Thus we consider it fair to use the above discussed generic approach operating with first-order slide parameters only. It is worth noting that the semi-empirical formulation applied in the present study was validated by a FNPF model (Grilli and Watts 1999).

Tsunami wave propagation is calculated using the finite difference model TUNAMI-N2 (Imamura et al. 1997). This nonlinear shallow water code uses the staggered leap-frog scheme for discretization of time and space. The shallow water approximation is fulfilled, as all wave lengths are much bigger than the water depth. Wave propagation is calculated on a 920×760 grid using a spatial step size Δx of 10 arc seconds (~309 m) and a time step Δt of 0.5 s. The influence of resolution was tested by variation of both Δx and Δt, further refinement did not change the results. Bathymetry is based on interpolated GEBCO data (IOC, IHO and BODC 2003).

Calculation of realistic tsunami run-up and inundations requires very high-resolution (~50 m) near-shore bathymetry and topography (see e.g., Titov and Synolakis 1997). In absence of high-resolution data (we employ GEBCO 1 nautic mile grid) we follow the approach similar to Geist and Parsons (2006) to estimate run-up heights. We extrapolate offshore wave amplitudes at water depths of about 100 m to final run-up values using the formula of Ward and Asphaug (2003): $R = A(d)^{4/5} \cdot d^{1/5}$, where $A(d)$ is the wave amplitude, measured at water depth d (Geist and Parsons 2006 implied constant amplification factor = 2). This formula was developed based on the conservation of wave energy flux and tested for both breaking and non-breaking waves (Ward and Asphaug

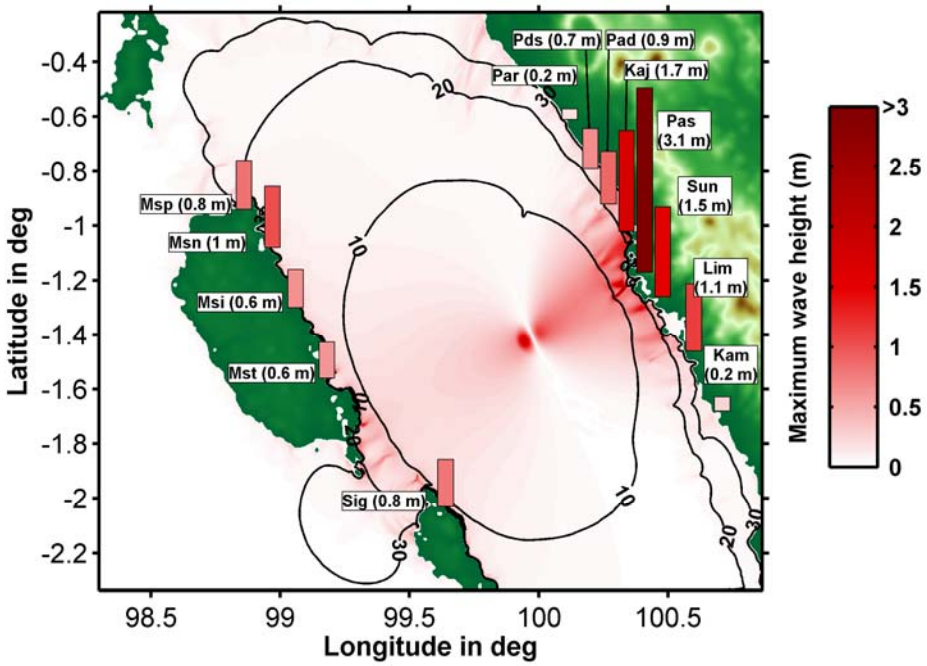

Figure 3 *Tsunami generated by slide A. Maximum wave height distributions after 2 hours, arrival times in minutes and estimated run-up along the coast. Abbreviations stand for following places (alphabetically ordered): Kaj: Kajuara, Kam: Kambang, Lim: Limaumanis, Msi: Muarasaibi, Msn: Muarasikabaluan, Msp: Muarasigep, Mst: Muarasiberut, Pad: Padang, Par: Pariaman, Pas: Pasar Sungainjalo, Pds: Padangsarai, Sig: Sigoisooinan, Sun: Sungaitalang.*

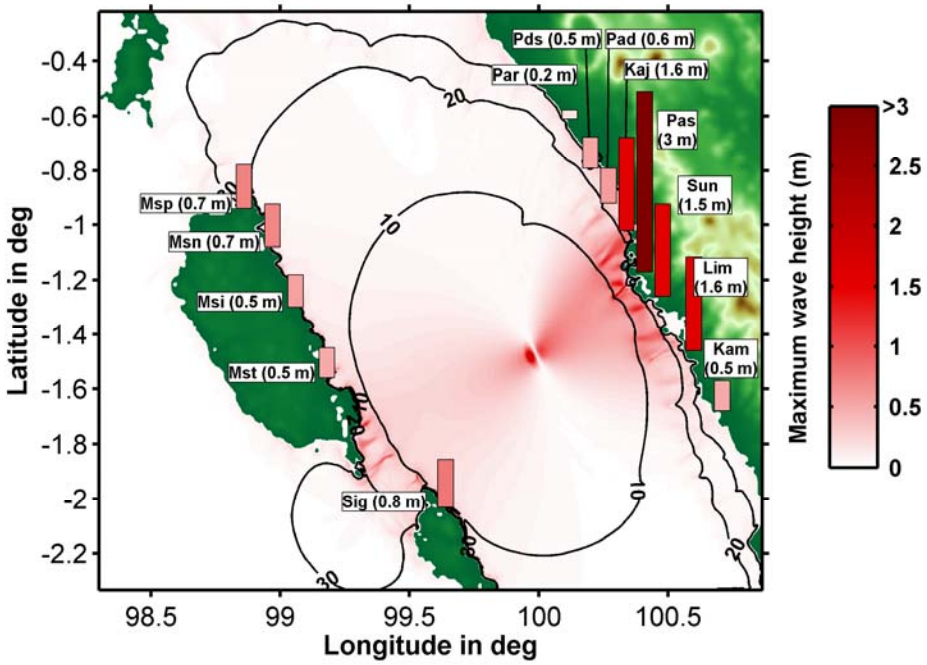

Figure 4 *Tsunami generated by slide B. Maximum wave height distributions after 2 hours, arrival times in minutes and estimated run-up along the coast. For abbreviated place names, see Figure 3.*

2003). Such approximation does not pretend to represent 'true run-up' which is extremely strong influenced by local bathymetry and topography. Instead, we refer to the results obtained with the above formula as effective 'estimated run-up heights'.

4.2 Results

First, we consider each slide independent of the others. Slide A induces a wave reaching Siberut after 20, and Padang after 25 minutes (Figure 3). The maximum wave height at the virtual gauge off Padang, in a water depth of 100 m, is 0.3 m. This corresponds to an estimated run-up height of about 1 m at Padang. The highest effective run-up of 3 m is found south of Padang, in Pasar Sungainjalo. Calculated run-up at Siberut Island does not exceed 1 m. The slightly smaller slide B shows similar results (Figure 4). It generates 3 m run-up in Pasar Sungainjalo as well as about half a meter in Padang and at Siberut. The third event, slide C, induces only a small tsunami. Although we do not take into account multiple stage failure, which would further reduce wave heights, effective estimated run-up heights do not exceed 0.3 m.

The next model assumes simultaneous failure of the events A and B. As the two landslides are located alongside, an earthquake that led to the failure of one slide might have also triggered the other. The natural worst case scenario hereby consists of the superposition of both initial wave forms at the same moment. This scenario yields a maximum effective run-up of nearly 4 m in Pasar Sungainjalo and about 2 m at Sungaitalang. Both places are located in a zone where run-up values are augmented by positive interference of the two slide-induced tsunamis (Figure 5). This is also the case

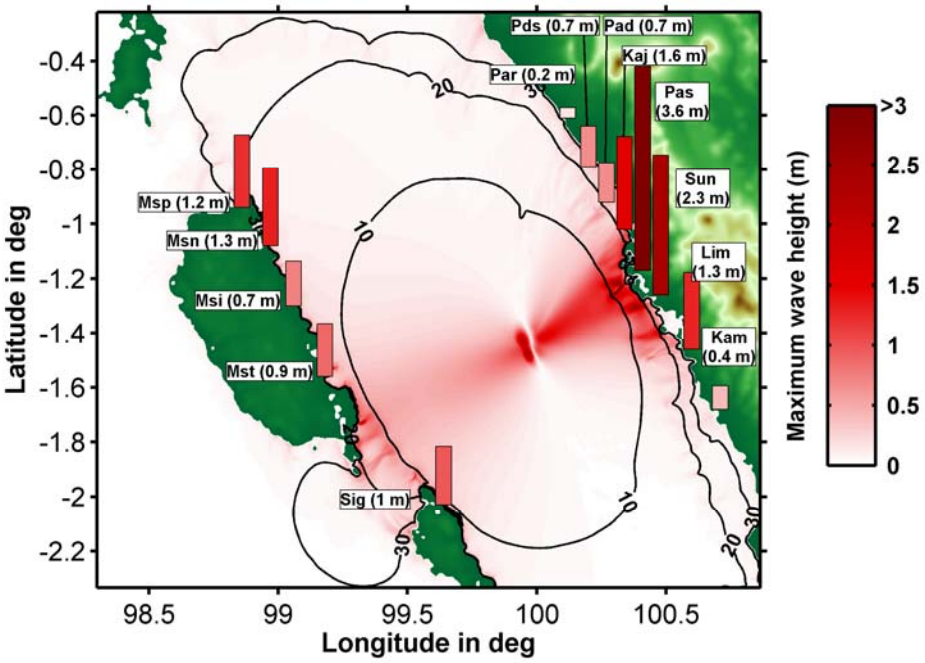

Figure 5 *Worst case tsunami generated by slides A and B simultaneously. Maximum wave height distributions after 2 hours, arrival times in minutes and estimated run-up along the coast. For abbreviated place names, see Figure 3.*

for Siberut Island, where calculated run-up values reach 1.3 m. However, some places do not experience strong interference. At Padang, for example, the run-up of the combined scenario is nearly identical to that for every single event.

The above run-up values are obtained without considering tidal oscillations. As high tides reach approximately 0.7 m above mean zero (UHSLC), the worst case run-up might be nearly 2 m at Padang and 3 to 4 m at locations south of Padang. Waves of this size are capable to endanger people and probably damage small vessels and structures near the coast line (Papadopoulos and Imamura 2001). Additionally, if slides are triggered by an earthquake, superposition of the waves to an earthquake tsunami is possible.

While slide geometry and travel distance of event A can be estimated from bathymetric data quite accurately, both length and travel distance of slide B are subjected to a higher uncertainty. Parameter studies show that this uncertainty could be responsible for run-up variations of ~20 % for slide A and ~50 % for slide B.

5. Spatial aspect for landslide hazard assessment

In section 4.2, we calculate tsunamis of given landslides and estimate whether they could have posed a danger for the city of Padang. In this section, we go a step further and investigate the tsunamigenic potential of a broad spectrum of hypothetical events in the Padang area. Hypothetical run-ups in Padang depend not only on the size of the landslide, but also on its geographical location in the Mentawai Basin. The latter determines not only the distance to Padang, but also submergence depth, slope angle, and slide direction - parameters which control tsunami generation by the following mechanisms:

a) Slide depth: Initial wave heights decrease for increasing depth. The reason lies in the dynamical build up of the wave. (Tinti et al. 2001, Fritz et al. 2004) The tsunami propagation velocity augments with water depth. If this velocity becomes larger than the speed of the submarine slide itself, the generated tsunami wave starts to spread out while the slide movement still modifies the water surface. Thus, with constant slide velocities, deeper slides generally cause smaller initial wave heights. A secondary effect is that for small slides, the ocean surface deformation appears to be attenuated with increasing water depth (Kajiura 1963; Tinti et al. 1999).

b) Slope angle: Larger slope angles facilitate the release of the slides potential energy. Hence, they cause higher slide velocities.

c) Slide direction: In the near-field, amplitudes are strongly influenced by the slide's direction: Landslides induce a large positive water wave in down slope direction and a somewhat smaller negative one in the up slope facing area. However, these waves interfere negatively in slope-parallel direction. This mechanism is responsible for vanishing values of maximum wave heights of Figures 3 and 4 in the slope-parallel zones.

d) Distance to Padang: The amplitudes of landslide tsunamis decay comparatively fast, due to geometrical spreading of the wave and the dipolar slide nature (Okal and Synolakis 2003). We regard the distance between slide and point of observation as a first-order parameter for the amplitude decay. The actual wave pattern, however, is usually influenced by bathymetrical focusing or defocusing effects (Satake 1988).

Location	Slide depth (m)	Slide direction (°)	Slope angle (°)	Distance to Padang (km)	Slide volume (km^3)
1	580	57	0.4	175	20
2	670	167	1	150	10
3	790	193	0.8	120	15
4	490	175	0.1	200	>25
5	880	79	1	145	15
6	1200	146	1.2	115	10
7	1400	222	2.5	90	20
8	670	232	1.2	60	15
9	310	242	0.9	35	15
10	490	336	0.1	200	>25
11	1490	98	0.9	120	15
12	1080	218	2.3	65	10
13	580	220	1.1	40	5
14	1380	78	3.1	125	15
15	1550	226	0.7	80	15
16	880	241	1.7	60	7
17	560	52	4.9	140	8
18	1510	13	0.9	120	15
19	1560	195	0.4	85	15
20	640	243	2.1	80	15
21	2100	259	0.1	225	>25
22	550	204	0.1	200	>25
23	860	62	1.8	140	15
24	1620	45	1	120	15
25	1020	228	4	105	20
26	3490	218	0.2	240	>25
27	1380	263	0.1	220	>25
28	1040	188	0.1	195	>25
29	660	221	0.1	175	>25
30	940	41	2.8	145	15
31	860	234	2.4	135	20
32	1290	64	1.7	165	25

Table 2 *Main parameters of scenarios that induce more than 2 m effective run-up in Padang. Please refer to Figure 6 for a map of slide location and their associated numbers. Slide direction is measured with respect to north, in clockwise direction. A graphical representation of the scenarios is depicted in Figure 6.*

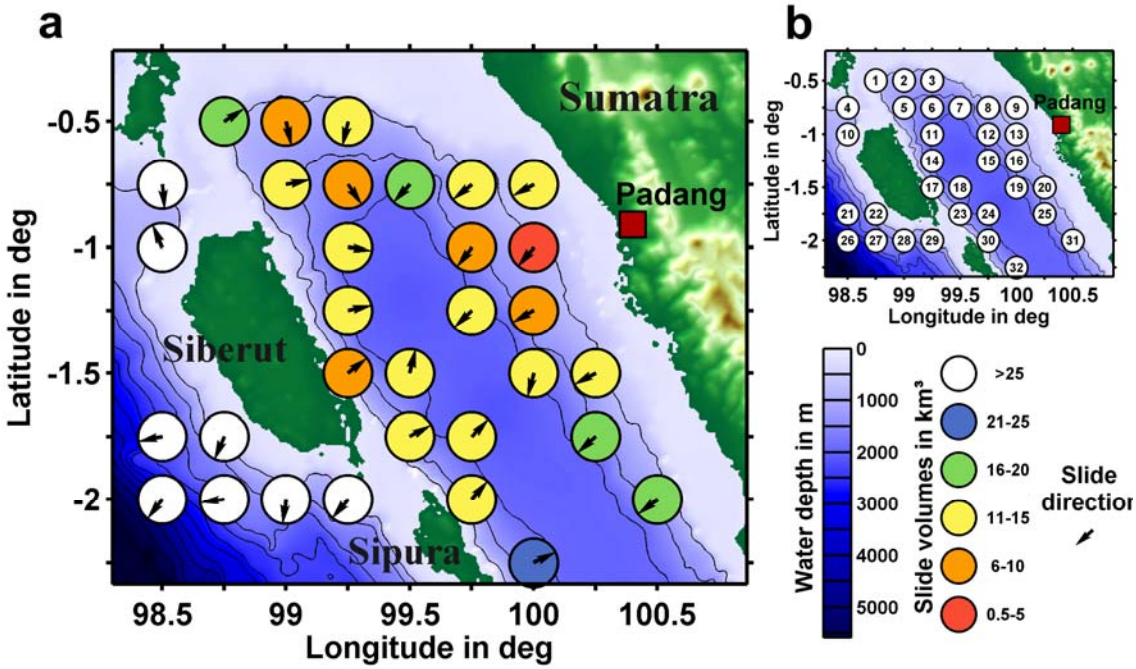

Figure 6 (a) *Resultant hazard assessment for landslide-generated tsunamis off Padang. Colored circles represent the location and the smallest volume of a landslide capable to generate 2 m effective run-up in Padang. Arrows inside the circles depict slide directions. Contour lines show water depths at 500 m intervals.* ***(b)*** *Associated scenario numbers.*

The main question we want to address is: how large must a submarine landslide at a given location be, in order to induce dangerous (> 2 m) run-up at Padang. Therefore, we systematically model landslides on a 0.25-degree structured grid off Padang (Figure 6b). We ignore locations at the bottom of the fore-arc basin due to vanishing slope angles as well as places of very shallow water depth, where the model applicability mentioned in section 4.1 is exceeded. At each of the 32 resulting positions, we simulate 14 landslides of different volumes, ranging from 0.5 to 25 km³. We prescribe the direction of motion to be down slope along the negative bathymetry gradient. In order to minimize the number of parameters, we consider events with radial symmetry and a constant width. These synthetic events follow properties of the real events A and B. Namely, we assume rotational slumping as fault mechanism, a slump width and length of 5 km and fix the center-of-mass travel distance to 2 km. Landslide thickness varies between 13 m and 640 m to reach slide volumes from 0.5 km³ to 25 km³, respectively.

Whether a landslide at a predefined location can induce a dangerous tsunami in Padang, is strongly dependent on its volume. Table 2 and Figure 6a show the smallest landslides, at each location, which generate more than 2 m run-up in Padang. An event at the same location, but with a larger volume will always generate a larger tsunami. Thus, the scenario with the smallest volume represents the lower end of the hazard potential at this position.

The general pattern of Figure 6a can be explained as follows. Slides at position 13 which locate in relatively small depth and whose upslope direction points towards Padang start to pose a danger even for very small volumes. For locations southwest of position 13, slide depths increase along with the distance towards Padang, necessitating larger failure volumes for a given final wave height. Even further southwest, on the outer slope of the fore arc basin, the slide direction reverses. Here, the large first positive wave reaches Padang. Thus, although the distance to Padang is significantly larger than on the northeast basin slopes, the critical volume remains comparable. Slides on the oceanic side of the Mentawai Islands do not pose any danger within the studied volume range of maximal 25 km³. Siberut Island and the fore-arc high reflect most of the wave energy into the open ocean and thereby shield the coast of Sumatra.

Within the complex overall pattern, the relevance of a single parameter like the slide direction is not obvious. Its relevance can be seen only by comparing two scenarios with otherwise similar slide parameters. Location 9 and 13, for instance, share comparable depth, slope angle and distance to Padang. Only the slide direction with respect to Padang is different, so that for slides at location 9, Padang is located in the above mentioned zone of negative interference. This results in a much larger necessary slide volume than for location 13. An analogue situation can be observed for position 6 and 7. Again, the slide direction is responsible for the apparent difference in critical volumes.

6. Conclusions

Three landslides have been detected in the Mentawai fore-arc basin, 70 km off Padang. Their volumes were estimated to be 0.7 km³, 0.5 km³ and 0.1 km³. The slides show small erosive features, so a recent failure can be excluded. We numerically modeled the generated tsunamis using a semi-empirical technique for the evaluation of initial wave height and characteristic wave length. Tsunami propagation was computed with a non-linear, finite difference, shallow water code. Finally, we applied an empirical law to calculate run-up at the coast. Our results show nearly 1 m effective run-up in Padang for the two largest events A and B. Maximum estimated run-up of about 3 m was calculated south of Padang, in Pasar Sungainjalo, which is located closer to the slide area. The third landslide did not generate a significant tsunami. Under high tide conditions, run-up would increase by roughly one meter. If the two large events happened simultaneously, the resulting tsunami waves would superpose, possibly reaching run-ups of up to 4 m. Finally, we performed a preliminary hazard assessment study for the city of Padang, answering the question of how large a submarine landslide at a given location has to be, in order to generate dangerous (> 2 m) run-up at Padang. Inside the fore-arc basin, dangerous scenarios exhibit volumes between 0.5 and 25 km³, while outside the basin volumes smaller than 25 km³ do not pose any danger for Padang. The main landslide parameters which control the hazard distribution of landslide-generated tsunamis are: volume, distance to Padang, water depth in the generation region and slide direction.

Acknowledgements

Data collection were conducted with grant 03G0189 (SUMATRA) of the Federal Ministry of Education and Research (BMBF), Germany. This is publication 24 of the

GITEWS project (German Indonesian Tsunami Early Warning System). The project is carried out through a large group of scientists and engineers from GeoForschungsZentrum Potsdam (GFZ) and its partners from DLR, AWI, GKSS, IFM-GEOMAR, UNU, BGR, GTZ, as well as from Indonesian and other international partners. Funding is provided by the German Federal Ministry for Education and Research (BMBF), grant 03TSU01. We thank two anonymous reviewers for their detailed and constructive comments.

References

Borrero JC, R Hidayat, Suranto, C Bosserelle, EA Okal (2007) Field survey and preliminary modeling of the near-field tsunami from the Bengkulu earthquake of 12 September 2007. Eos Trans AGU. 88(52), Fall Meet. Suppl., Abstract U54A-04

Chlieh M, JP Avouac, K Sieh, DH Natawidjaja, J Galetzka (2008) Heterogeneous coupling of the Sumatran megathrust constrained by geodetic and paleogeodetic measurements. J Geophys Res. Doi:10.1029/2007JB004981

Fritz HM, WH Hager, HE Minor (2004) Near field characteristics of landslide generated impulse waves. J Waterway Port Coastal Ocean Eng. Doi: 10.1061/(ASCE)0733-950X(2004)130:6(287)

Fritz HM, W Kongko, A Moore, B McAdoo, J Goff, C Harbitz, B Uslu, N Kaligeris, V Titov, CE Synolakis (2007) Extreme run-up from the 17 July 2006 Java tsunami. Geophys Res Abstr. 9:10765

Geist EL, T Parsons (2006) Probabilistic Analysis of Tsunami Hazards. Nat Hazards. 37:277-314

Grilli ST, P Watts (1999) Modeling of waves generated by a moving submerged body. Applications to underwater landslides. Eng Anal Bound Elem. 23:645-656

Grilli ST, S Vogelmann, P Watts (2002) Development of a 3D numerical wave tank for modeling tsunami generation by underwater landslides. Eng Anal Bound Elem. 26:301-313

Grilli ST, P Watts (2005) Tsunami generation by submarine mass failure. I: Modeling, experimental validation, and sensitivity analyses. J Waterway Port Coastal Ocean Eng. 131(6):283-297

Hamilton EL (1985) Sound velocity as a function of depth in marine sediments. J Acoust Soc Am. 78(4):1348-1355

Hamzah L, NT Puspito, F Imamura (2000) Tsunami Catalog and Zones in Indonesia. J Nat Disaster Sci. 22(1):25-43

Harbitz CB (1992) Model simulations of tsunamis generated by the Storegga slides. Mar Geol. 105:1-21

Imamura F, MMA Imteaz (1995) Long waves in two-layers: Governing equations and numerical model. J Sci Tsunami Hazards. 13:3-24

Imamura F, N Shuto, C Goto, Y Ogawa (1997) IUGG/IOC Time Project IOC Manuals and Guides No.35, (UNESCO)

IOC, IHO and BODC (2003) Centenary Edition of the GEBCO Digital Atlas, British Oceanographic Data Centre, Liverpool

Kajiura K (1963) The leading wave of a tsunami, Bull Earthq Res Inst. 41:535-571

Lavigne F, C Gomez, M Giffo, P Wassmer, C Hoebreck, D Mardiatno, J Prioyono, R Paris (2007) Field observations of the 17 July 2006 Tsunami in Java. Nat Hazards Earth Syst Sci. 7:177-183

Lorito S, F Romano, A Piatanesi, E Boschi (2008) Source process of the September 12, 2007, MW 8.4 southern Sumatra earthquake from tsunami tide gauge record inversion. Geophys Res Lett. Doi:10.1029/2007GL032661

Lynett P, PLF Liu (2002) A numerical study of submarine-landslide-generated waves and run-up. Proc R Soc A. 458:2885

Lynett P, PLF Liu (2005) A numerical study of the run-up generated by three-dimensional landslides. J Geophys Res. Doi: 10.1029/2004JC002443

Lückge A, M Mohtadi, C Rühlemann, G Scheeder, A Vink, L Reinhardt, M Wiedicke (2009) Monsoon versus ocean circulation controls on paleoenvironmental conditions off southern Sumatra during the past 300,000 years. Paleoceanography. Doi: 10.1029/2008PA001627

Masson DG, CB Harbitz, RB Wynn, G Pedersen, F Løvholt (2006) Submarine landslides: processes, triggers and hazard prediction. Phil. Trans. R. Soc. A, 364:2009-2039

Matsumoto T (2007) An underwater landslide or slump on an active submarine fault - A possible source of a devastating tsunami? Eos Trans AGU. 88(52), Fall Meet. Suppl., Abstract S53A-1018

McCloskey J, A Antonioli, A Piatanesi, K Sieh, S Steacy, S Nalbant, M Cocco, C Giunchi , JD Huang, P Dunlop (2008) Tsunami threat in the Indian Ocean from a future megathrust earthquake west of Sumatra. Earth Planet Sci Lett. 265:61-81

Moran K, D Tappin (2006) SEATOS 2005 Cruise Report: Sumatra Earthquake and Tsunami Off shore Survey (SEATOS). 92 pp. (Online) available at http://ocean.oce.uri.edu/seatos.

Natawidjaja DH, K Sieh, M Chlieh, J Galetzka, BW Suwargadi, H Cheng, RL Edwards, JP Avouac, SN Ward (2006) Source parameters of the great Sumatran megathrust earthquakes of 1797 and 1833 inferred from coral microatolls. J Geophys Res Solid Earth. Doi:10.1029/2005JB004025

Neben S, C Gaedicke (2006) Cruise Report, BGR Cruise SO189 Leg 1, Project SUMATRA, The Hydrocarbon System of the Sumatra Forearc, Bundesanstalt für Geowissenschaften und Rohstoffe, 126 pp.

Okal EA, CE Synolakis (2003) A Theoretical Comparison of Tsunamis from Dislocations and Landslides. Pure Appl Geophys. 160:2177-2188

Papadopoulos GA, F Imamura (2001) A proposal for a new tsunami intensity scale, ITS 2001 Proceedings, Session 5, Number 5-1

Pelinovsky E (2001) Analytical Models Of Tsunami Generation By Submarine Landslides. In: AC Yalçiner, E Pelinovsky, E Okal, C E Synolakis (eds) Submarine Landslides and Tsunamis, 2003 Kluwer Academic Publishers, pp 111-128

Rynn J (2002) A preliminary assessment of tsunami hazard and risk in the indonesian region. Sci Tsunami Hazard. 20(4):193

Satake K (1988) Effects of Bathymetry on Tsunami Propagation: Application of Ray Tracing to Tsunamis. Pure Appl Geophys. 126(1):27-36

Susilohadi S, C Gaedicke and A Ehrhardt (2005) Neogene structure and sedimentation history along the Sunda forearc basins off southwest Sumatra and southwest Java Marine Geology. Mar Geo. Doi: 10.1016/j.margeo.2005.05.001.

Sweet S and EA Silver (2003) Tectonics and Slumping in the Source Region of the 1998 Papua New Guinea Tsunami from Seismic Reflection Images. Pure Appl Geophys. 160:1945-1968

Synolakis CE, JP Bardet, JC Borrero, HL Davies, EA Okal, EA Silver, S Sweet and DR Tappin (2002) The slump origin of the 1998 Papua New Guinea Tsunami. Proc R Soc Lond. A 458:763-789

Synolakis CE, L Kong (2006) Runup Measurements of the December 2004 Indian Ocean Tsunami. Earthq Spectr. 22(S3):S67-S91

Tappin DR, P Watts, GM McMurtry, Y Lafoy, T Matsumoto (2001) The Sissano, Papua New Guinea tsunami of July 1998-offshore evidence on the source mechanism. Mar Geol. 175:1-23

Tinti S, E Bortolucci, C Vannini (1997) A Block-Based Theoretical Model Suited to Gravitational Sliding. Nat Hazards. 16:1-28

Tinti S, E Bortolucci, A Armigliato (1999) Numerical simulation of the landslide-induced tsunami of 1988 on Vulcano Island, Italy. Bull Volcanol. (1999) 61 :121–137

Tinti S, E Bortolucci, C Chiavettieri (2001) Tsunami Excitation by Submarine Slides in Shallow-water Approximation. Pure Appl Geophys. 158: 759-797

Titov VV, CE Synolakis (1997) Extreme inundation flows during the Hokkaido-Nansei-Oki tsunami Geophys Res Lett. 24(11):1315-1318

Tsuji Y, F Imamura, H Matsutomi, CE Synolakis (1995a) Field Survey of the East Java Earthquake and Tsunami of June 3, 1994. Pure Appl Geophys. 144(3/4):839

Tsuji Y, H Matsutomi, F Imamura, M Takeo (1995b) Damage to Coastal Villages due to the 1992 Flores Island Earthquake Tsunami. Pure Appl Geophys. 144(3/4), 481

UHSLC (University of Hawai, Sea Level Center) 2008, http://ilikai.soest.hawaii.edu/

Ward SN, E Asphaug (2003) Asteroid impact tsunami of 2880 March 16. Geophys J Int. 153:F6-F10

Watts P, ST Grilli, D Tappin, GJ Fryer (2005) Tsunami generation by submarine mass failure. II: Predictive equations and case studies. J Waterway Port Coastal Ocean Eng. 131(6):298-310

Yuk D, SC Yim, PLF Liu (2006) Numerical modeling of submarine mass-movement generated waves using RANS model. Comput Geosci. 32:927–935